Protein Science (1999), *8*:1765–1772. Cambridge University Press. Printed in the USA.
Copyright © 1999 The Protein Society

X-ray crystallographic analysis of the structural basis for the interactions of pokeweed antiviral protein with its active site inhibitor and ribosomal RNA substrate analogs

I.V. KURINOV,[1] D.E. MYERS,[1] J.D. IRVIN,[2] AND F.M. UCKUN[1]

[1]Hughes Institute, 2665 Long Lake Road, Roseville, Minnesota 55113
[2]SouthWest Texas State University, 601 University Drive, San Marcos, Texas 78666

(RECEIVED March 3, 1999; ACCEPTED May 14, 1999)

Abstract

The pokeweed antiviral protein (PAP) belongs to a family of ribosome-inactivating proteins (RIP), which depurinate ribosomal RNA through their site-specific N-glycosidase activity. We report low temperature, three-dimensional structures of PAP co-crystallized with adenyl-guanosine (ApG) and adenyl-cytosine-cytosine (ApCpC). Crystal structures of 2.0–2.1 Å resolution revealed that both ApG or ApCpC nucleotides are cleaved by PAP, leaving only the adenine base clearly visible in the active site pocket of PAP. ApCpC does not resemble any known natural substrate for any ribosome-inactivating proteins and its cleavage by PAP provides unprecedented evidence for a broad spectrum N-glycosidase activity of PAP toward adenine-containing single stranded RNA. We also report the analysis of a 2.1 Å crystal structure of PAP complexed with the RIP inhibitor pteoric acid. The pterin ring is strongly bound in the active site, forming four hydrogen bonds with active site residues and one hydrogen bond with the coordinated water molecule. The second 180° rotation conformation of pterin ring can form only three hydrogen bonds in the active site and is less energetically favorable. The benzoate moiety is parallel to the protein surface of PAP and forms only one hydrogen bond with the guanido group of Arg135.

Keywords: active site interactions; ribosome inactivating proteins; RNA substrate analogs; X-ray crystallography

Pokeweed antiviral protein (PAP) from the leaves of the pokeweed plant, *Phytolacca americana*, is a naturally occurring 29 kDa single chain ribosome inactivating protein (RIP), which catalytically inactivates both prokaryotic and eukaryotic ribosomes. The therapeutic potential of PAP has gained considerable interest in recent years due to the clinical use of native PAP as the active moiety of immunoconjugates against cancer and AIDS (Irvin & Uckun, 1992).

PAP is a site-specific RNA N-glycosidase that enzymatically removes a single adenine base (A4324) from a highly conserved, surface exposed "α-sarcin" loop of the large rRNA species in eukaryotic (28S rRNA) and prokaryotic (23S rRNA) ribosomes (Irvin, 1983; Endo et al., 1988). This catalytic depurination of the α-sarcin loop, which is positioned in immediate vicinity of the peptidyltransferase center within the 50 S subunit of *Escherichia coli* ribosomes, impairs the interactions between ribosomes and elongation factor 2 (EF–2), resulting in irreversible inhibition of protein synthesis at the EF–2 mediated translocation step (Dallal & Irvin, 1978; Gessner & Irvin, 1980).

PAP has also been shown to effectively inhibit the replication of several plant and animal viruses including poliovirus, herpes simplex virus, cytomegalovirus, influenza virus, and human immunodeficiency virus (HIV)-1 (Zarling et al., 1990; Irvin & Uckun, 1992). The molecular mechanism of the antiviral activity of PAP is under active investigation (Bonness et al., 1994; Chaddock et al., 1994, 1996; Hur et al., 1995; Tumer et al., 1997, 1998; Xu et al., 1998). Besides its ability to inhibit viral protein synthesis, PAP is also capable of directly depurinating viral RNA (Barbieri et al., 1997). Furthermore, PAP also displays viral RNA-specific effects in vivo and has been shown to inhibit ribosomal frameshifting and retrotransposition, a molecular mechanism used by many RNA viruses to produce Gag-Pol fusion proteins (Tumer et al., 1998).

Wild-type PAP was crystallized and its structure refined to a 2.5 Å resolution at room temperature (Monzingo et al., 1993). To date, no structural information has been reported regarding the interaction of PAP with its natural substrates. A working hypothesis regarding the structural basis for the N-glycosidase activity of PAP was proposed based on the structural similarities of the active sites of PAP and a more extensively analyzed RIP, ricin A-chain (Katzin et al., 1991; Kim & Robertus, 1992; Monzingo & Robertus, 1992). This hypothesis was predicated upon the supposition that PAP and ricin A-chain are identical in their enzymatic activity and provides no explanation for the more broad-spectrum N-glycosidase activity of PAP (Hartley et al., 1991; Barbieri et al., 1993; Marchant & Hartley, 1995).

Reprint requests to: F.M. Uckun, Hughes Institute, 2665 Long Lake Road, Roseville, Minnesota 55113; e-mail: fatih_uckun@ih.org.

In this paper, we report a low temperature X-ray structure analysis and supporting modeling studies of the interactions of PAP with nucleotide analogs of its natural rRNA substrate. In particular, the dinucleotide adenyl(3′–5′)guanosine (ApG) and trinucleotide adenyl-cytosine-cytosine (ApCpC) were co-crystallized with PAP and computer modeling studies were performed to elucidate the structural basis of the interactions between PAP and its ligands. The low temperature X-ray data extended to a 1.9 Å resolution allowing a more detailed interpretation of the enzyme-substrate complexes. It was observed that PAP had cleaved both ApG and ApCpC, and only adenine base was visible in the active site pocket. The cleavage of ApCpC, which does not resemble any known natural substrate (GAGAG motif in a RNA stem-loop (Endo et al., 1988; Marchant & Hartley, 1995; Chen et al., 1998)) for any RIP, provides experimental evidence for a broad spectrum N-glycosidase activity of PAP toward any adenine containing single-stranded RNA. To better understand the interaction of the PAP active site with adenine containing oligonucleotides, we also performed a co-crystallization with pteoric acid (PTA), which is a weak inhibitor of ricin (Yan et al., 1997).

Results and discussion

PAP crystals belong to the triclinic space group with two molecules in the unit cell. There are no large conformational differences between the two PAP molecules of the asymmetric unit because of noncrystallographic symmetry restraints imposed during the crystallographic structure refinement. The root-mean-square deviation (RMSD) was 0.07 Å for the main-chain and 0.16 Å for side-chain atoms between two PAP monomers. Overall conformation and mode of interaction of all studied ligands were the same in two monomers. For the purpose of structural comparison, the average values of the two models will be used for subsequent analysis.

Analogous to other RIPs (ricin A-chain, trichosantin, momordin), PAP has a well-defined secondary structure: eight α-helices and a β-sheet composed of six strands. Comparison of our room temperature PAP structure at the resolution 2.0 Å with the published PAP structure at resolution 2.5 Å (Monzingo et al., 1993) shows better stereochemistry with RMSDs of 0.008 Å for bond lengths and 1.6° for angles, as compared to 0.027 Å and 3.4°, respectively, for 1PAF structure. A direct comparison of our structure with the published structure (Protein Data Bank (PDB) code 1PAF) did not show a significant discrepancy for backbone conformation and RMSD for the main-chain atoms was only 0.34 Å. Only a few atoms differ more than 0.9–1.0 Å. The comparison of the residues in the active site region showed even less discrepancy with RMSD of 0.24 Å.

Low temperature studies

In an attempt to prolong the crystal life and improve the resolution limits, we performed a low temperature study of PAP crystals. This is especially important for a triclinic unit cell. The first noticeable effect of lowering temperature was a decrease of unit cell parameters. The relative volume reduction caused by the lowering of temperature was approximately 2.4% and the corresponding actual volume change was 3,060 Å^3 per unit cell. The observed unit cell volume change was smaller than that reported for RNAse (4.7%) (Tilton et al., 1992) or myoglobin (5%) (Frauenfelder et al., 1987). The thermal expansion of the protein can also be parameterized in terms of the radius of gyration. Since the radius of gyration is proportional to the moment of inertia, it gives a rough estimation of protein volume. The radius of gyration calculated for all nonhydrogen atoms of PAP decreased by about 1.9% (this corresponds to a 5.7% decrease of the volume of the appropriate ellipsoid). A similar behavior was observed for the accessible surface area of PAP. A 3.2% decrease in the accessible surface area shows that the roughness of the PAP surface does not increase with freezing and reflects the overall shrinkage of protein. A direct comparison of low temperature (LT) and room temperature (RT) structures shows no significant structural differences except for the usual thermal expansion of the protein substance. Two monomers in the unit cell changed their relative position upon freezing—the relative sliding and pivoting of the monomers occurred to form a more dense packing at low temperature. After rigid-body rotation and translation (which are different for two monomers), both backbones were nearly identical (Fig. 1), which could be a consequence of abundant secondary structure elements. RMSD for the main-chain atoms was 0.30 Å and none of the main-chain atoms, except C- and N-terminus, had deviations more than 1 Å. A comparison between LT and RT structures is even smaller when comparing a secondary structure elements or active site region of the protein. No large conformational reorientations of side chains were observed; only some large and/or disordered side chains became more ordered at LT. We were unable to identify any definitive alternate conformations in PAP at LT. A lower overall *B*-factor and a smaller range in *B*-factor profile were observed for the LT structures. Although the temperature factor plotted against the residue number (Fig. 2) showed a similar pattern for LT and RT structures, there were many indications of a nonuniform decrease of the *B*-factor upon crystal freezing.

PAP interactions with substrate analogs

The structural element of rRNA targeted by PAP (Hartley et al., 1991; Barbieri et al., 1993) is a very conserved stem-loop structure containing the GAGAG motif (the cleaved adenine is underlined). Therefore, we co-crystallized PAP with adenyl-guanosine to elucidate the interactions of PAP with its rRNA substrates. Crystals of PAP-ApG complex have the same space group and very similar unit cell parameters (see Table 1). The initial $2F_o - F_c$ electron density map for PAP complexed with ApG showed continuous density in the active site pocket, which slightly protruded along the protein surface from the PAP active site. This density was initially fitted with ApG having the best and energetically favorable conformation from our modeling studies (see Materials and methods). Initially all atoms of ApG were assigned *B*-factors of 20 Å^2, close to mean value for the active site residues. The next round of structure refinement (slow cooling annealing, positional, and individual *B*-factor refinement) lead to an increase of the *B*-factor for guanosine group up to 40 Å^2 and the *B*-factor for the adenosine group to ~25 Å^2. The uneven distribution of *B*-factor on phosphate backbone excluded a consideration of static disorder for the guanosine group. The omit electron density maps showed continuous electron density covering only the adenine group and half of the sugar; the rest of the molecule is covered by separate peaks, more similar to water peaks (Fig. 3). So, we assumed that ApG was cleaved by PAP during the rather long crystallization setup and only the adenine moiety was left bound in the active site pocket. This hypothesis was clearly confirmed by the next round of structure refinement where we retained only the adenine base and in-

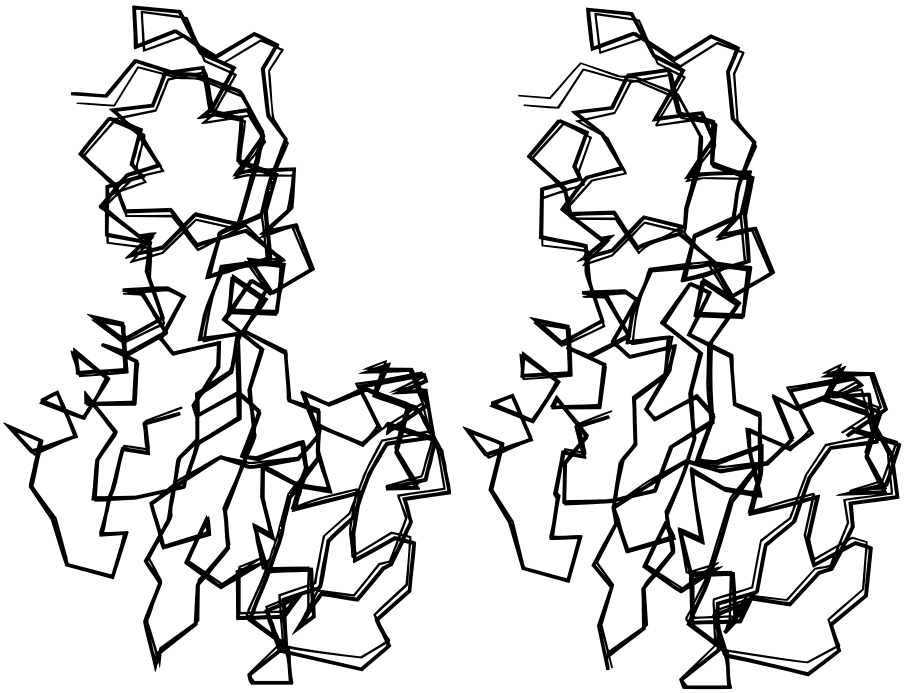

Fig. 1. A Cα traces of PAP A-monomers at RT and LT following superimposition of their respective main-chain coordinates. The trace of the RT PAP structure is drawn with thicker line. Comparison of B-monomers shows a similar pattern.

cluded water molecules in the distinctive peaks shown on the previous electron omit map density in place of guanidine and the phosphate linker. Although the resulting difference in *R*-free factor is not substantial (<0.3%), the final omit electron density map clearly covered only the adenine base in the active site and surrounding water molecules without any ambiguity.

Figure 4 shows the binding site region of the omit map for the PAP-adenine complex. The mode of adenine interaction with PAP active site residues is essentially identical to that seen previously in ricin complexed with ApG (Monzingo & Robertus, 1992). The adenine ring is sandwiched between tyrosines 72 and 123. N6 of adenine donates a hydrogen bond to the carbonyl oxygen of Val73 (distance 3.4 Å), N1 receives a hydrogen bond from the amino nitrogen of Val73 (distance 2.9 Å). Arg179 can donate a hydrogen bond to N3 (distance 2.6 Å) and N7 is hydrogen bonded to the carbonyl oxygen of Ser121 (2.7 Å). The only noticeable difference between this complex and the complex of PAP with formycin (Monzingo et al., 1993) is the orientation of Tyr72. Tyr72 in the PAP-adenine complex does not appear to have altered its torsion angle χ_1 upon ligand binding as was observed in the PAP-formycin complex. Orientation of the Tyr72 in the PAP-adenine complex remains the same as in ligand-free form of PAP.

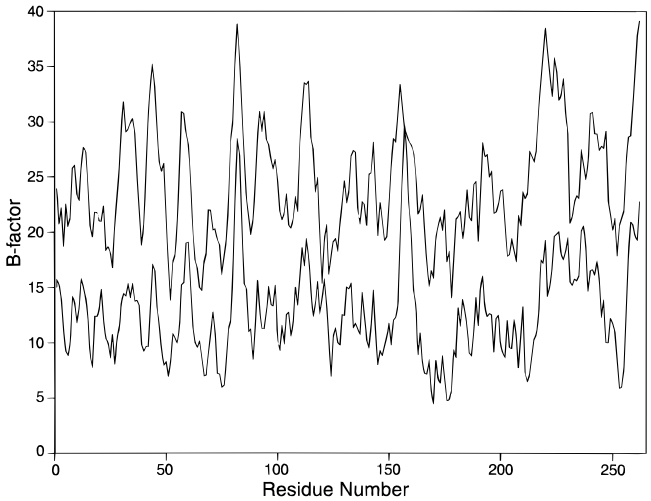

Fig. 2. Main-chain atoms averaged *B*-factor dependence on the residue number for ligand-free PAP structure at RT (upper line) and LT (lower line).

The absence of an electron density for the guanosine ring suggests that the enzyme remains active during the crystallization setup. Our study of the PAP-ApG complex follows the earlier study of a PAP complex with formycin-monophosphate (Monzingo et al., 1993). Formycin-monophosphate could not be cleaved by PAP because of the C-C bond between pyrazolepyrimidine and ribose sugar. Ricin A-chain is a more extensively studied RIP and its complexes with adenosine-monophosphate (Weston et al., 1994) and ApG (Monzingo & Robertus, 1992) were described. It was shown that adenosine-monophosphate is cleaved by ricin A-chain (only adenine was seen in the active site). The overall orientation of the dinucleotide ApG with adenine bound in the active site is definitively the same in the ApG-ricin complex and PAP. However, small differences in surface topology near the active site pocket may account for different rates of ApG depurination by PAP and ricin (ApG is not considered as a substrate for ricin in kinetics studies by (Chen et al., 1998)).

Table 1. *Details of data collection and refinement*

	Wild-type PAP RT	Wild-type PAP LT	PAP-ApG complex	PAP-ApCpC complex	PAP-PTA complex
Unit (*a*)	49.47	48.68	48.48	48.64	48.19
Cell (*b*)	49.47	49.09	49.03	49.08	48.50
Å (*c*)	64.77	64.56	63.87	64.39	63.92
α	68.73	67.95	68.79	68.75	68.85
β	81.12	82.90	81.05	82.55	81.78
γ	64.13	65.37	63.88	64.87	64.62
Unit cell volume ($Å^3$)	132,920	129,860	127,080	129,620	128,480
R-merge (%)	4.8	5.9	6.0	6.6	6.9
Resolution limit for refinement	2.0	2.1	2.0	2.1	2.1
Completeness of data used for refinement (%)	91.0	87.0	89.4	87.9	85.3
R-factor (%)	19.9	20.8	23.0	24.5	23.0
Number of water molecules	478	479	448	414	541
Protein *B*-factor (A^2)	23.9	13.3	19.9	20.1	16.2

Taking into consideration the broad specificity of PAP toward ribosomes from different sources and its very high affinity to the adenine base, we tried to explore the binding and interaction of PAP with the tri-nucleotide ApCpC. ApCpC is not known to be a natural substrate for PAP or RIPs, so we expected the PAP–ApCpC complex would at least help to characterize the interaction with phosphate backbone.

ApCpC was co-crystallized with PAP in the same manner as ApG with the same space group and unit cell parameters. However, the examination of the omit map density in the active site pocket again showed the presence of only an adenine base, without any indications of an electron density corresponding to two cytidines. This very unusual result supports the notion that PAP has a high affinity toward adenine-containing oligonucleotides without a high degree of selectivity toward the closest nucleotide residues in the sequence.

PAP complex with pteroic acid (PTA)

To further study the interaction of PAP with ligands, we co-crystallized PAP with pteoric acid. PTA was already shown to be a weak inhibitor of ricin A-chain and X-ray studies demonstrated the putative structure of PTA bound to ricin (Yan et al., 1997). Because there are no known natural inhibitors of PAP, and it is shown that ricin A-chain and PAP share the same active site structure, we decided to use PTA as a possible ligand for PAP. Our

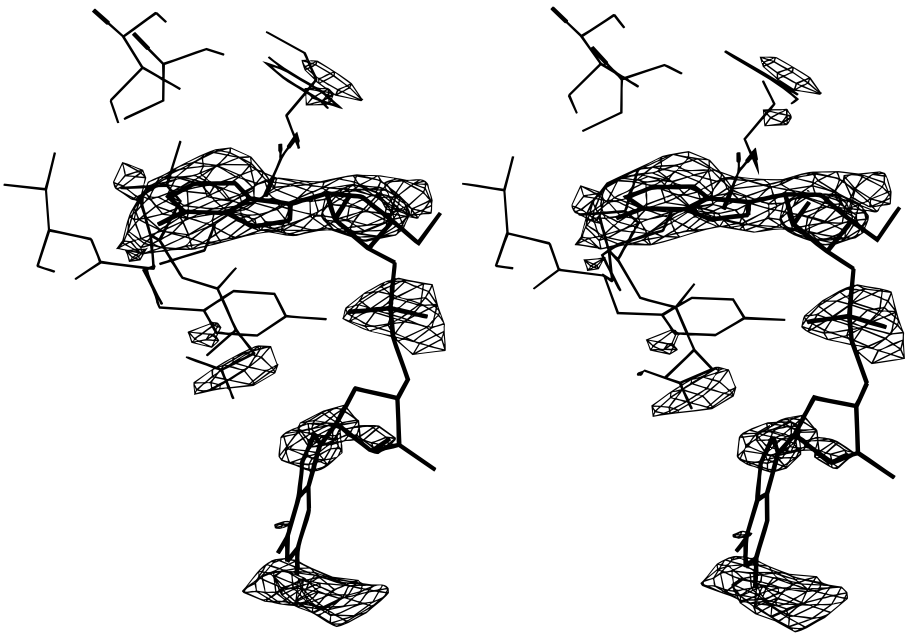

Fig. 3. Omit electron density map ($F_o - F_c$) for PAP-ApG complex at LT. ApG was omitted for map calculations. Model for ApG is drawn in bold. The map is contoured at 1.5σ.

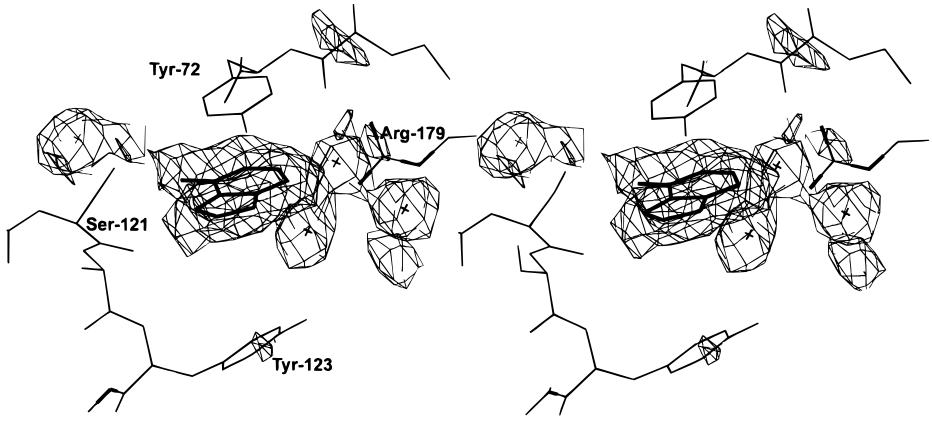

Fig. 4. Omit electron density map ($F_o - F_c$) for PAP-adenine complex at low temperature. Adenine base was omitted for map calculations. The map is contoured at 2σ.

preliminary kinetics data had revealed a decrease of ribosome depurination in the presence of PTA (F. Rajamohan & F.M. Uckun, unpubl. results).

Crystals of PAP complexed with PTA remained isomorphous to ligand-free PAP (see Table 1). Initially PTA was manually docked into the active site pocket in the conformation derived from our computer simulation results. After a crystallographic refinement, the omit electron density map clearly showed a continuous electron density covering the whole PTA molecule. The same orientation of bound PTA was observed in two PAP monomers. Although our modeling studies did not show the preferred orientation of PTA complexed with PAP, the initial electron density was sufficient to properly position the PTA benzoic acid outside the active site pocket. After the second cycle of refinement, the ambiguity concerning the orientation of the main ring in the active site pocket persisted. Therefore, two more cycles of refinement were performed with two different orientation of the pterin ring (180° flipping). The precision of the electron density maps was not enough to discriminate between the two conformations (Fig. 5). However, the mode of interaction of two conformation differ considerably, and we assume that only one of the conformations has the best pattern of hydrogen bonding of pterin ring with the active site residues. The best orientation of the pterin ring reveals four hydrogen bonds to protein atoms (backbone N of Val73, two bonds with Oγ of Ser121 and Oγ of Ser175), and one bond is mediated by strongly bound water molecule, WAT133 (details are displayed on Fig. 6). The second orientation of pterin ring can form only three hydrogen bonds, which are less optimal than those formed in the first orientation. The second orientation of pterin ring inside the PAP active site corresponds to the conformation observed in PTA-ricin complex (Yan et al., 1997), and its interactions with active site residues are similar to those of adenine. We observed a rotation of Tyr72 ring to accommodate pterin ring in the active site.

The benzoate moiety of PTA lies parallel to the protein surface, and its carboxyl oxygen is linked to the guanido group of Arg135. It is apparent that the benzoate group of PTA does not significantly

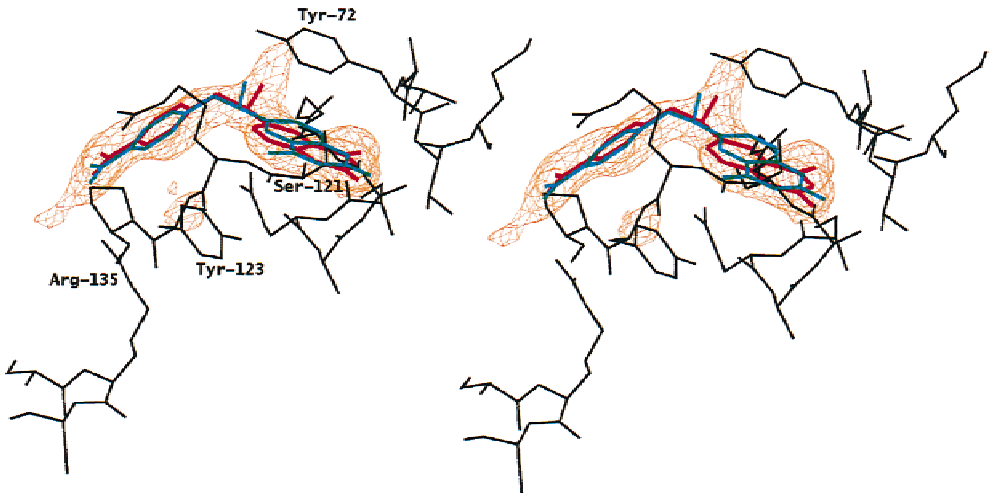

Fig. 5. Omit electron density map ($F_o - F_c$) for PAP-pteoric acid complex at low temperature. PTA was omitted for map calculations. The map is contoured at 2σ. Two different conformations (180° rotation) of pterin ring (shown in blue and red) are superimposed on the figure. The conformation having the more favorable interaction profile is shown in blue.

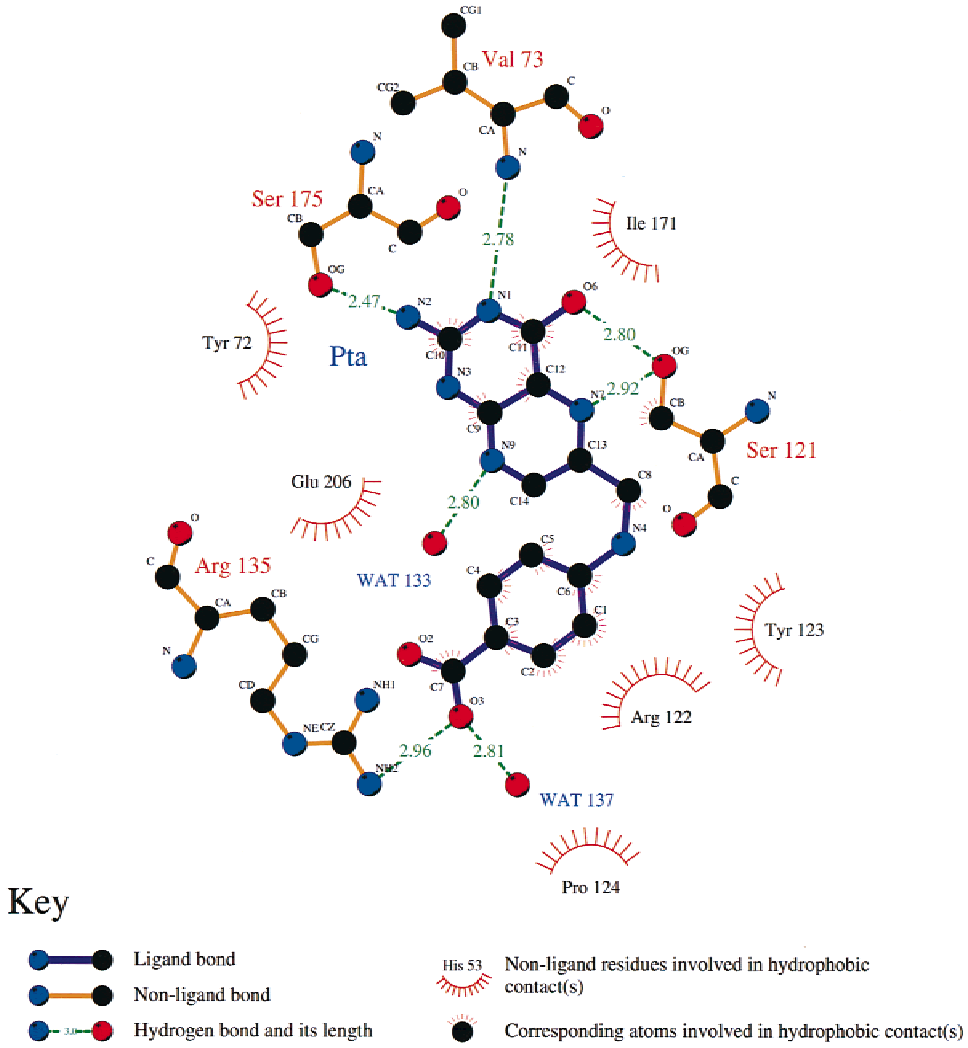

Fig. 6. Details of interaction of pteroic acid with active site residues of PAP. The figure was drawn using LIGPLOT (Wallace et al., 1995).

contribute to the binding of PTA to PAP. The overall orientation of the benzoate group is clearly different from its orientation in the ricin-PTA complex (Yan et al., 1997; Fig. 7). The benzoate ring of PTA is bent around Tyr80 of ricin (Tyr72 of PAP) and its carboxyl oxygen is near Asn78 (Asn70 of PAP). Although Asn78 of ricin and Asn70 of PAP occupy the same position, PTA complexed with PAP cannot assume the same orientation as PTA complexed with ricin because of the different orientation of the tyrosine ring. Side-chain Tyr72 of PAP has more restricted conformational freedom because of the neighboring Ser121. The ricin residue, which correspond to Ser121 of PAP, is Gly121, which has no interactions with the tyrosine ring. Because of the flexible links between pterin and benzoate rings, the latter can adopt a conformation toward Arg135, which is located on the opposite side of the active site from Asn70. In fact, the benzoate rings complexed with both ricin and PAP appear to be bound in a long concave region, which may accommodate a single strand of a natural RNA substrate.

An experimentally obtained three-dimensional structure of PAP complexed with a larger substrate analogue consisting of a stem-loop structure would be likely to provide valuable information about the details of mechanism of PAP enzymatic activity.

Materials and methods

Protein purification and crystallization

PAP was extracted from spring leaves of pokeweed and purified to homogeneity as previously described (Myers et al., 1991). Just before the crystallization setup PAP was repurified on a MonoS cation-exchange column (Pharmacia Biotech, Piscataway, New Jersey) and filtered through 0.22 μm filter. ApG, ApCpC, and pteoric acid were purchased from Sigma (St. Louis, Missouri) and were used without additional modifications.

PAP crystals were obtained from a concentrated PAP preparation (15–20 mg/mL) by the vapor diffusion method within 2–3 weeks using "hanging drop" experiments with 16–18% PEG 4000 and 0.1 M $CaCl_2$ (50 mM Tris-HCl buffer pH = 8) at room temperature. Crystals of PAP-ApG and PAP-ApCpC complexes were grown in the above solution with the addition of 5 mM ApG or ApCpC. PAP-PTA crystals were grown from same solution but saturated with PTA; otherwise the crystallization conditions were identical. Unit cell parameters, details of data collection, and refinement are presented in Table 1. To prolong the crystal lifetime and increase

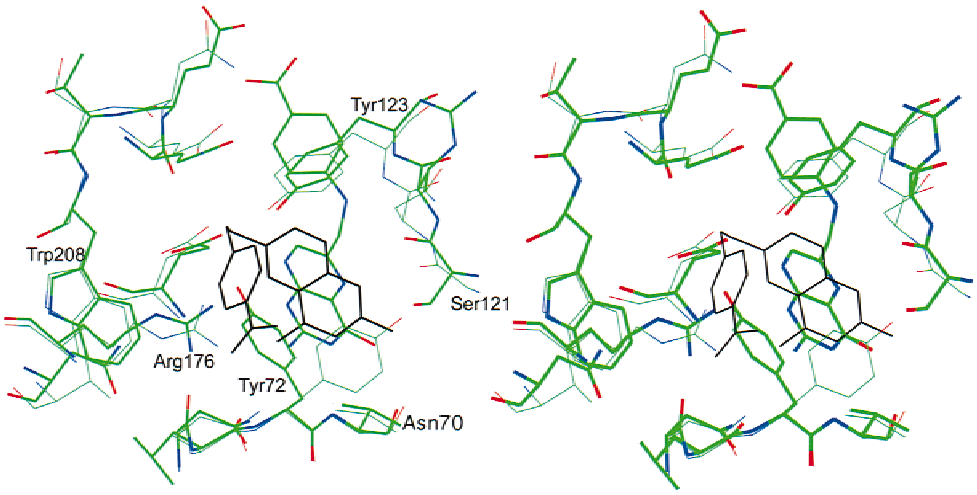

Fig. 7. Stereo view of the superimposition of PAP and ricin (Yan et al., 1997) active site residues with bound PTA. Ricin atoms are shown in thin lines; PTA is black. PAP with bound PTA is drawn in thick lines.

the resolution limits, low temperature studies were done using a 25% PEG4000 solution as a cryoprotectant, and the protein crystal was flash-frozen under a liquid nitrogen stream. Upon freezing, PAP crystals usually exhibited a mosaicity increase of 0.2–0.5°. Low temperature studies (~100 K) were done using the X-stream system from MSC (Woodlands, Texas). Diffraction data were collected on a Rigaku RaxisIY imaging plate. The X-ray source was a copper Rigaku RU300H generator with a double mirror system operating at 50 kV and 100 mA. The crystal-to-detector distance was 150 mm, and the crystal (in one or two different orientations) was rotated around the spindle axis with images collected over 1.5° to a resolution of 1.9–2.0 Å. Data were evaluated using the bioTex processing software (MSC) or HKL package (DENZO and SCALEPACK (Otwinowski & Minor, 1998)). The completeness of data sets at low temperature was over 85% when the completeness of the data set in the last resolution shell was 70–80%. The real resolution of the data, used for structure refinement, was estimated to be 2.0–2.1 Å (see Table 1) taking into consideration the completeness of the last resolution shell, I/σ ratio and *R*-merge values.

Model refinement

The atomic coordinates of the refined PAP (PDB access code 1PAF) were used for the initial crystallographic phasing and refinement of the new PAP structure. All calculations were done using X-PLOR (version 3.1) (Brünger, 1992). All data with $I/\sigma > 2$ and a low-resolution limit of 8 Å were used for structure refinement. Nonpolar hydrogens were implicitly included in their associated heavy atoms. There were two PAP monomers per unit cell, and they are approximately related by a twofold symmetry nearly coincident with the crystallographic a-axis. During the crystallographic refinement we imposed noncrystallographic symmetry (NCS) restraints on the atom position and *B*-factors of two monomers, including ligand models. At the early stage of the crystallographic refinement, strong NCS restraints were imposed to keep the structure of two molecules close and not to increase the free *R*-factor. As the refinement progressed, the values of the effective energy constant for the positional restraints between two monomers were relaxed from 300 to 60 kcal/mol/Å^2 for the main-chain atoms and 30 kcal/mol/Å^2 for the side-chain atoms. Complete removal of NCS restraints led to a small increase of *R*-free factor.

A few cycles of slow-cooling annealing (3,500 → 100 K), positional and restrained isotropic temperature factor refinements were followed by visual inspection of electron density maps, including omit maps, coupled with a manual model building (when necessary) using the graphics program CHAIN (Sack, 1988). A ligand-free PAP structure at room temperature (RT) was used as a starting point for the refinement of every PAP structure at low temperature (LT). Strong stereochemical restraints were imposed during the crystallographic refinement and all final PAP structures possessed a similarly good stereochemistry with an RMSD of ~0.008 Å for bond lengths and ~1.4° for angles. The RMSD between two molecules before and after the final round of refinement was 0.06 Å. The quality of the stereochemistry of the final protein structure was assessed with the PROCHECK package (Laskowski et al., 1993). The Ramachandran plot shows no residues in disallowed regions (data not shown).

All procedures during crystal growing, data collection and processing as well as structure refinement were identical for all studied complexes, which simplified the comparison of the final structures and eliminated some of the systematic errors. As a better guide to the quality of the structure, the values of the free *R*-factor were monitored during the course of the crystallographic refinement. The final value of free *R*-factors did not exceed the overall *R*-factor by more than 7%.

The refined coordinates of wild-type PAP at low temperature and PAP complexes with adenine and pteoric acid have been deposited in the PDB (access codes 1QCG, 1QCI, and 1QCJ, respectively).

Ligand docking modeling

The molecular docking of ligands and estimation of the interaction scores were done using a *Fixed Docking* procedure in the *Affinity*

program within the InsightII modeling software (InsightII User Guide, 1996). We created a definitive binding set of PAP residues in the active site pocket to move as a 3.5 Å shell around the manually docked ligand during the energy minimization. The number of final docking positions was set to 20, although finally only 3–5 promising positions were identified. The calculations used a CVFF force-field in the *Discovery* program and a Monte Carlo strategy in the *Affinity* program. Each energy-minimized final docking position of the ligand was evaluated using the interactive score function in the *Ludi* module. Ludi score includes contribution of the loss of translational and rotational entropy of the fragment, number and quality of hydrogen bonds, and contributions from ionic and lipophilic interactions to the binding energy.

Acknowledgments

This material is based in part upon work sponsored by the Defense Advanced Research Projects Agency under Grant N65236-99-1-5422. The content does not necessarily reflect the position or policy of the U.S. Government, and no official endorsement should be inferred.

References

Barbieri L, Batelli MG, Stirpe F. 1993. Ribosome-inactivating proteins from plants. *Biochem Biophys Acta 1154*:237–282.

Barbieri L, Valbonesi P, Bonora E, Gorini P, Bolognesi A, Stirpe F. 1997. Polynucleotide: Adenosine glycosidase activity of ribosome-inactivating proteins: Effect on DNA, RNA and poly(A). *Nucl Acids Res 25*:518–522.

Bonness MS, Ready MP, Irvin JD, Mabry TJ. 1994. Pokeweed antiviral protein inactivates pokeweed ribosomes: Implications for the antiviral mechanism. *Plant J 5*(2):173–183.

Brünger AT. 1992. *X-PLOR (version 3.1). A system for X-ray crystallography and NMR*. New Haven, Connecticut: Yale University Press. 405 pp.

Chaddock JA, Lord JM, Hartley MR, Roberts LM. 1994. Pokeweed antiviral protein (PAP) mutations which permit *E. coli* growth do not eliminate catalytic activity towards prokaryotic ribosomes. *Nucl Acids Res 22*(9):1536–1540.

Chaddock JA, Monzingo AF, Robertus JD, Lord JM, Roberts LM. 1996. Major structural differences between pokeweed antiviral protein and ricin A-chain do not account for their differing ribosome specificity. *Eur J Biochem 235*(1–2):159–166.

Chen XY, Link TM, Schramm VL. 1998. Ricin A-chain: Kinetics, mechanism and RNA stem-loop inhibitors. *Biochemistry 37*(33):11605–11613.

Dallal JA, Irvin JD. 1978. Enzymatic inactivation of eukaryotic ribosomes by the pokeweed antiviral protein. *FEBS Lett 89*:257–259.

Endo Y, Tsurugi K, Lambert JM. 1988. The site of action of six different ribosome-inactivating proteins from plants on eukaryotic ribosomes: The RNA N-glycosidase activity of the proteins. *Biochem Biophys Res Commun 150*(3):1032–1036.

Frauenfelder H, Hartmann H, Karplus M, Kuntz ID Jr, Kuriyan J, Parak F, Petsko GA, Ringe D, Tilton RF Jr, Connolly ML, Max N. 1987. Thermal expansion of a protein. *Biochemistry 26*(1):254–261.

Gessner SL, Irvin JD. 1980. Inhibition of elongation factor 2-dependent translocation by the pokeweed antiviral protein and ricin. *J Biol Chem 255*:3251–3253.

Hartley MR, Legname G, Osborn R, Chen Z, Lord JM. 1991. Single-chain ribosome inactivating proteins from plants depurinate *Escherichia coli* 23S ribosomal RNA. *FEBS Lett 290*(1–2):65–68.

Hur Y, Hwang DJ, Zoubenko O, Coetzer C, Uckun FM, Tumer NE. 1995. Isolation and characterization of pokeweed antiviral protein mutations in *Saccharomyces cerevisiae*: Identification of residues important for toxicity. *Proc Natl Acad Sci USA 92*(18):8448–8452.

InsightII User Guide. 1996. San Diego, California: MSI.

Irvin JD. 1983. Pokeweed antiviral protein. *Pharmacol Ther 21*:371–387.

Irvin JD, Uckun FM. 1992. Pokeweed antiviral protein: Ribosome inactivation and therapeutic applications. *Pharmacol Ther 55*(3):279–302.

Katzin BJ, Collins EJ, Robertus JD. 1991. Structure of ricin A-chain at 2.5 Å. *Proteins 10*(3):251–259.

Kim Y, Robertus JD. 1992. Analysis of several key active site residues of ricin A chain by mutagenesis and X-ray crystallography. *Protein Eng 5*(8):775–779.

Laskowski RA, MacArthur MW, Moss DS, Thornton JM. 1993. PROCHECK: A program to check the stereochemical quality of protein structures. *J Appl Crystallogr 26*:283–291.

Marchant A, Hartley MR. 1995. The action of pokeweed antiviral protein and ricin A-chain on mutants in the alpha-sarcin loop of *Escherichia coli* 23S ribosomal RNA. *J Mol Biol 254*(5):848–855.

Monzingo AF, Collins EJ, Ernst SR, Irvin JD, Robertus JD. 1993. The 2.5 Å structure of pokeweed antiviral protein. *J Mol Biol 233*(4):705–715.

Monzingo AF, Robertus JD. 1992. X-ray analysis of substrate analogs in the ricin A-chain active site. *J Mol Biol 227*(4):1136–1145.

Myers DE, Irvin JD, Smith RS, Kuebelbeck VM, Uckun FM. 1991. Production of a pokeweed antiviral protein (PAP)-containing immunotoxin, B43-PAP, directed against the CD19 human B lineage lymphoid differentiation antigen in highly purified form for human clinical trials. *J Immun Methods 136*:221–237.

Otwinowski Z, Minor W. 1998. Processing of X-ray diffraction data collected in oscillation mode. *Methods Enzymol 276*:307–325.

Sack JS. 1988. CHAIN: A crystallographic modeling program. *J Mol Graph 6*:224–225.

Tilton RF Jr, Dewan JC, Petsko GA. 1992. Effects of temperature on protein structure and dynamics: X-ray crystallographic studies of the protein ribonuclease-A at nine different temperatures from 98 to 320 K. *Biochemistry 31*(9):2469–2481.

Tumer NE, Hwang DJ, Bonness M. 1997. C-terminal deletion mutant of pokeweed antiviral protein inhibits viral infection but does not depurinate host ribosomes. *Proc Natl Acad Sci USA 94*(8):3866–3871.

Tumer NE, Parikh BA, Li P, Dinman JD. 1998. The pokeweed antiviral protein specifically inhibits Ty1-directed +1 ribosomal frameshifting and retrotransposition in *Saccharomyces cerevisiae*. *J Virol 72*(2):1036–1042.

Wallace AC, Laskowski RA, Thornton JM. 1995. LIGPLOT: A program to generate schematic diagrams of protein-ligand interactions. *Protein Eng 8*(2):127–134.

Weston SA, Tucker AD, Thatcher DR, Derbyshire DJ, Pauptit RA. 1994. X-ray structure of recombinant ricin A-chain at 1.8 Å resolution. *J Mol Biol 244*(4):410–422.

Xu J, Meng AX, Hefferon KL, Ivanov IG, Abouhaidar MG. 1998. Effect of N-terminal deletions on the activity of pokeweed antiviral protein expressed in *E. coli*. *Biochimie 80*(12):1069–1076.

Yan X, Hollis T, Svinth M, Day P, Monzingo AF, Milne GW, Robertus JD. 1997. Structure-based identification of a ricin inhibitor. *J Mol Biol 266*(5):1043–1049.

Zarling JM, Moran PA, Haffar O, Sias J, Richman DD, Spina CA, Myers DE, Kuebelbeck V, Ledbetter JA, Uckun FM. 1990. Inhibition of HIV replication by pokeweed antiviral protein targeted to CD 4+ cells by monoclonal antibodies. *Nature 347*(6288):92–95.